NUCL SCI TECH (2016) 27:92
DOI 10.1007/s41365-016-0083-9

A novel heating area design of temperature-jump microfluidic chip for synchrotron radiation solution X-ray scattering

Yi-Wen Li[1,2] · Feng-Gang Bian[1] · Jie Wang[1]

Received: 20 January 2016 / Revised: 29 February 2016 / Accepted: 2 March 2016 / Published online: 11 July 2016

Abstract In this paper, we present a novel design scheme of temperature-jump (T-jump) area for microfluidic device. Numerical simulation and experimental research of thermal characteristics of the solution in microchannels is completed. Numerical simulation of the temperature-jump microchannel is analyzed to study the heat transfer characteristics by comparing performance of three proposed configurations. Calculation of the power requirement is discussed in the dimensional design of microheater. Temperature-sensitive fluorescent dye is applied to investigate the temperature field of microchannel heated by a designed microheater. It is found that the T-jump microfluidic device can provide rapid heating for solutions with strong convection heat transfer ability.

Keywords Synchrotron radiation · Solution X-ray scattering · Microfluidic chip · Temperature-jump

1 Introduction

The temperature-jump (T-jump) technique is of great significance for elucidating reaction mechanisms. Perturbed by a rapid temperature change, the reaction system adjusts to a new equilibrium. During the equilibrium shift, the order of reaction steps and the rate of each step can be inferred from intensity of the light absorbed or fluoresced, or from the electrical conductivity [1]. Synchrotron radiation facility, which generated extremely strong X-ray beams, brought dramatic improvement in the kinetic observation by reducing the measurement time [2, 3].

Several approaches can be used to induce the T-jump. Joule heating produced by a fast electrical discharge of capacitor is a common method to rapidly increase the temperature of electrolyte solution [4–6]. Non-aqueous solvents, however, are ruled out due to the limit that the sample solution must be of high electrical conductivity. Without strict requirements, microwave heating can increase the temperature of solution which is held in cell mounted in a waveguide cavity [7, 8]. Also, laser technique is widely applied to generate a sudden rise in temperature of solvent by vibration absorption of a near-infrared laser pulse [9–12]. These heating apparatuses are usually complex and inconvenient when they are coupled with an endstation of synchrotron radiation. Simplifying both device structure and operation is therefore of paramount importance for combing T-jump technique with synchrotron radiation.

We have designed and constructed a novel microfluidic thermal system which enables rapid temperature change and is capable of fitting in the beam lines of synchrotron radiation facilities [13, 14]. The design and experimental results of the T-jump area of microfluidic chip will be elaborated in this paper. In the following sections, the design and fabrication of microchannel and heater, experimental method and measurement results are presented. For further understanding about the thermal characterization of the microfluidic chip, a computational fluid dynamics

This work was supported by the National Basic Research Program of China (No. 2011CB911104).

✉ Feng-Gang Bian
bianfenggang@sinap.ac.cn

✉ Jie Wang
wangjie@sinap.ac.cn

[1] Shanghai Institute of Applied Physics, Chinese Academy of Sciences, Zhangjiang Campus, Shanghai 201204, China

[2] University of Chinese Academy of Sciences, Beijing 100049, China

software ANSYS CFX is used to analyze heat transfer performance of microchannel with different configurations. The temperature field in microchannel is characterized by measuring the temperature dependence on fluorescence intensity of fluorescent dye [15–18].

2 Design and fabrication

2.1 The microfluidic chip

The microfluidic chip is shown schematically in Fig. 1. It consists of the reservoir channel, T-jump channel and sample detection channel. The microchannels were fabricated in a 2-mm-thick PMMA substrate by micromill technique. The reservoir channel, 1 mm (w) × 0.8 mm (h), is in an invariable temperature environment by an external thermoelectric cooler. To ensure a constant flow rate and heating efficiency, the T-jump channel is of a trapezoid–rectangle–trapezoid shape of 11 mm (w) × 0.1 mm (h). The sample detection channel is a 1 mm (w) × 1 mm (h) × 30 mm (l) groove, being sealed on both sides by 20-μm-thick Kapton film that allows X-ray beams to pass through. Adhered to the substrate is a 1-mm-thick PMMA cover plate, with two holes for connecting the channel ends to Telflon tubing and a pumping system (Hamilton, Switzerland) that provides a steady flow rate for the microfluidics.

2.2 The T-jump channel

The area where the T-jump channel connects the reservoir channel forms a sudden dimensional change, hence enlarging the area of active heating. Different configurations of the T-jump channel were proposed (Fig. 2). Three-dimensional steady-state analysis models were built to evaluate performance of the three types of channels, and their heat transfer characteristics were analyzed by fluid dynamics analysis software ANSYS CFX. The Navier–Stokes and continuity equations were solved by coupling with heat transfer equations under the following boundary

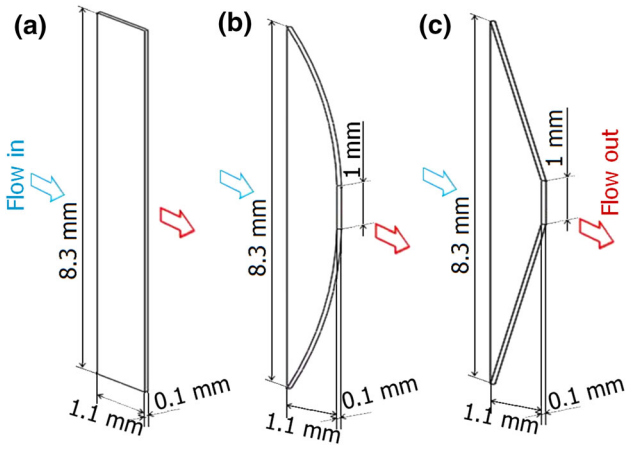

Fig. 2 Schematic view of T-jump microchannels. **a** Rectangular, **b** semielliptic, **c** trapezoid

conditions: (1) constant mass flow rate at microchannel inlet and 1 atm pressure at microchannel outlet; (2) constant front wall heat flux and adiabatic wall for others; (3) specific temperature of inlet fluid; (4) no-slip condition at the walls; and (5) incompressible fluid.

CFD analysis of the T-jump channels was investigated using water as working fluid. The flow characteristic was evaluated by the Reynolds number (Re) calculated by Eq. (1)

$$Re = \rho v D/\mu, \tag{1}$$

where ρ is the fluid density, v is the average fluid velocity, μ is the fluid viscosity and D is the hydraulic diameter defined as

$$D = 2ab/(a+b), \tag{2}$$

where a is the channel width and b is the channel height. In CFD analysis, the flow behavior is in laminar regime with Reynolds number below 2000. For the range of flow rate used in this work, Re is not larger than 20. The heat transfer characteristic was analyzed the Nusselt number (Nu) as

$$Nu = hD/\lambda, \tag{3}$$

where h is the heat transfer coefficient and λ is the thermal conductivity of fluid.

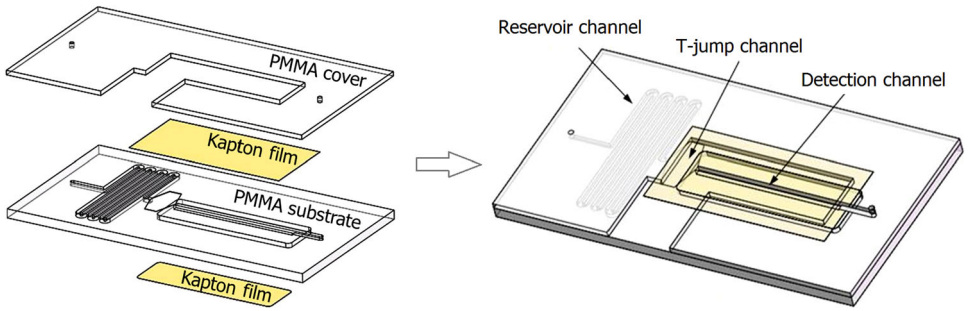

Fig. 1 Schematic 3-D view of the T-jump microfluidic chip

To compare performance of the three microchannel configurations, CFD analysis was conducted under the inlet flow rate of 10 μL/s at 35 C and heat flux of 70 kW/m^2. Under these conditions, the heat is transferred to the fluid by forced convection heat transfer. Figure 3 shows the Nusselt number as a function of inlet flow temperature in rectangle, semiellipse and trapezoid T-jump channels. Comparing the three sets of data, one sees that *Nu* of the trapezoid channel is the highest of all the channels. Although the *Nu* of trapezoid channel decreases slightly with increasing temperature, it keeps a strong microscale effect. The results of simulations at different heat fluxes and flow rates are similar. This shows that the channel geometry has great effect on heat transfer characteristics of microchannels. That the trapezoid channel performs the best in heat transfer can be attributed to the constant change of cross-sectional area. Due to the steady contraction of cross-sectional area, the flow in trapezoid channel experiences thermally developing laminar flow with significant entrance effect. In addition, the structure leads to some perturbation that aids to improve local heat transfer coefficient in the laminar flow.

2.3 The microheater

Considering thermal efficiency and non-disposable recyclability, a Pt film heater line is used. It is independent of the microfluidic chip, fastened on the PMMA substrate. When an electrical current passes through the resistance heater, the heat generated is transferred to the fluid in the microchannel. In this case, two main points, power generation and electromigration, should be taken into account in designing the dimensions of the heater [19]. The amount of heat, Q, transferred to the microfluidics can be estimated by

$$Q = Cm\Delta T, \tag{4}$$

where C is the specific heat capacity, m is the mass flow, and ΔT is the temperature change of fluid. To be specific, it can also be expressed in terms of power requirement

$$P\eta = Cm_r\Delta T, \tag{5}$$

where P is the power consumption of heater, η is the thermal efficiency, m_r is the mass flow rate of microfluidics.

The resistance of the heater, R_H, is given by

$$R_H = V^2/P, \tag{6}$$

where V is the supply voltage. The dimensions of the Pt film heater can be determined by Eq. (7)

$$R_H = \rho_f l/(wt), \tag{7}$$

where l, w and t are length, width and thickness of the Pt film heater, respectively, and ρ_f is resistivity of the Pt film which is different from bulk Pt owing to influence of mean free path of electrons.

In this study, the power source for heater was generated by a digital DC power supply (0–60 V), the thermal efficiency η was estimated at 20 % conservatively, the Pt film was 200 nm thick, and the mass flow rate of fluid was 10 mg/s. Resistivity of the Pt film was 2.8 × 10^{-7} Ω m [20], and specific heat capacity of water is 4200 J kg^{-1} K^{-1}. Finally, the temperature increment of the fluid are presented as a function of width–length ratio of the Pt film heater line

$$\Delta T = \alpha w/l, \tag{8}$$

where α is a coefficient determined by

$$\alpha = V^2\eta t/(Cm_r\rho_f) \tag{9}$$

Figure 4 shows temperature increment of the passing flow as a function of the width–length ratio at different applied voltages. The temperature increment rises with the width–length ratio and the applied voltage. The range of temperature increment of the fluid in the channel at a certain range of applied voltage can be decided by the

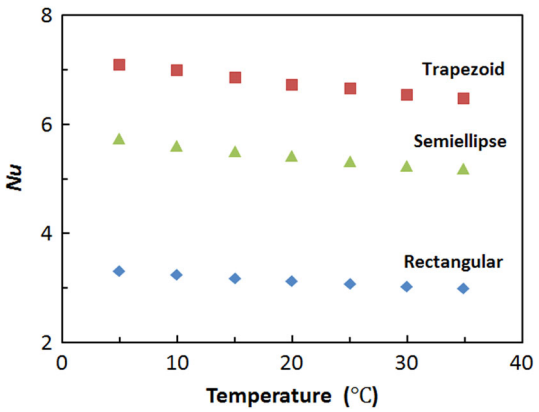

Fig. 3 Correlation of Nusselt number with inlet temperature

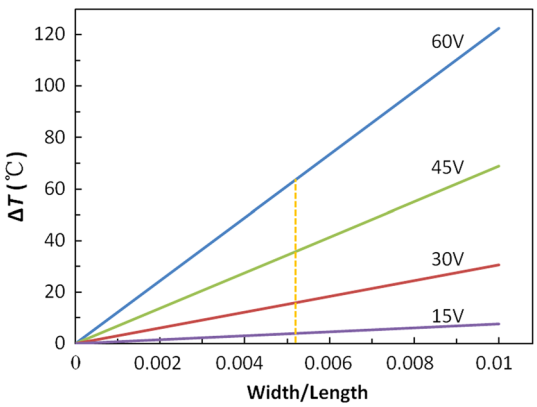

Fig. 4 Temperature increment versus width–length ratio of the Pt film heater line at different applied voltages. The *orange dash marks* the width–length ratio we used in the design

width–length ratio to optimize the heater performance. We chose the width–length ratio was 0.0052 in this design.

Another issue is the transport of metallic atoms in conductor, which is driven by the interaction with electrons of passing current. This electromigration decreases reliability of thin-Pt-film electronic component at a current density up to 10^7 A/cm^2 [21], which shall be the limit of current density of the heater line. Therefore, a zigzag heater line, spaced 100 μm apart with width of 200 μm, was designed and located at the trapezoid T-jump channel (Fig. 5). With the use of lift-off technique, 50 nm Cr and 200-nm-thick thin Pt film were deposited on a 1-mm-thick glass substrate. The room temperature resistance of the heater, including lead wires, is roughly 300 Ω.

3 Results and discussion

3.1 Fluorescence measurement

Temperature-dependent fluorescence dye, rhodamine B, was used in temperature measurements. The fluorescence intensity of rhodamine B was measured and converted to temperature value according to the calibrated intensity–temperature curve. Prior to the measurement, rhodamine B (Sigma Aldrich, USA) was dissolved into 15 mmol/L Na_2CO_3 buffer. Filtered with a 0.2-μm-syringe filter, the final concentration of rhodamine B was 87 μmol/L. Fluorescence imaging was performed using a CCD camera (DP71, Olympus, Japan) and commercial fluorescence microscope (BX51, Olympus, Japan) equipped with a standard green fluorescence filter set. The exposure time was set to a constant manually, and the white/black balance control was remained off throughout measurements.

In order to correlate the fluorescence intensity with temperature, a microfluidic chip integrated with a Pt100 thermal sensor (Heraeus, Germany) along the microchannel was fabricated. The microfluidic chip was fixed onto a silicone rubber thermostat (homemade) for a constant temperature environment of rhodamine B solution which was injected into the microchannel. The fluorescence images of the channel filled with dye solution were obtained at different temperatures of 25–80 °C. To eliminate effects of background fluorescence inhomogeneity, background and room temperature images were acquired preferentially during the measurement. For each pixel, the intensity value was subtracted with the background and normalized with the intensity value at room temperature.

3.2 Fluorescence experimental results

As shown in Fig. 6, the correlation between intensity and temperature was established. The normalized intensity at each temperature was averaged from multi-measurement. The data can be fitted by Eq. (10), with $R^2 = 0.998$:

$$T = 120.17 - 238.01I + 232.77I^2 - 88.16I^3, \quad (10)$$

where T is the temperature of rhodamine B solution and I is the normalized fluorescence intensity of rhodamine B solution after background subtraction.

The calibrated intensity–temperature relationship was used to explore thermal changes of fluid in the T-jump microchannel. A flow of the rhodamine B solution was continuously injected into the microfluidic chip and dissipated the heat energy provided by external Pt heater as described in Sect. 2.3. By changing the voltage applied on the Pt heater, various temperature increments of the fluid at each flow rate were obtained from the fluorescent images at the outlet of T-jump microchannel according to the intensity–temperature calibration curve.

The fluorescence inside the microchannel was measured at flow rates of 5 and 10 μL/s at 25 °C of fluid in the reservoir channel. The temperature change, ΔT, was determined as a function of power input. Figure 7 shows the results at power input of 0.22–2.1 W at 5 and 10 μL/s, with $\Delta T = 4-30$ °C at the outlet of T-jump microchannel. As can be seen, higher heater power generated larger temperature increment.

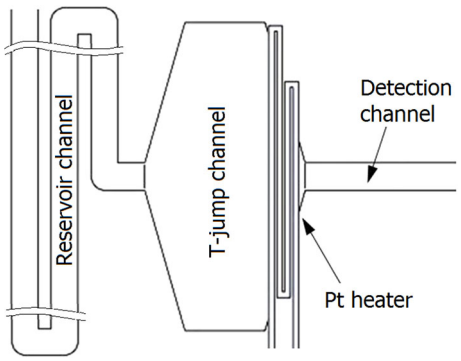

Fig. 5 Schematic drawing of the Pt heater on the microchannel

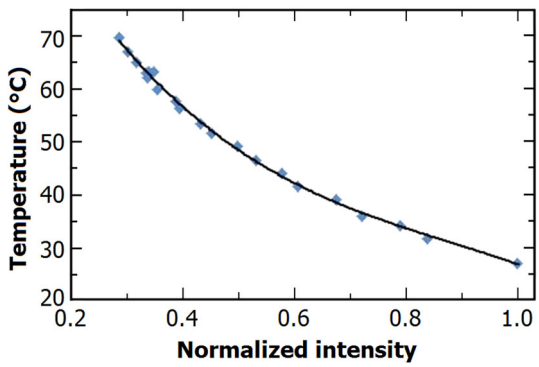

Fig. 6 The calibrated intensity–temperature curve

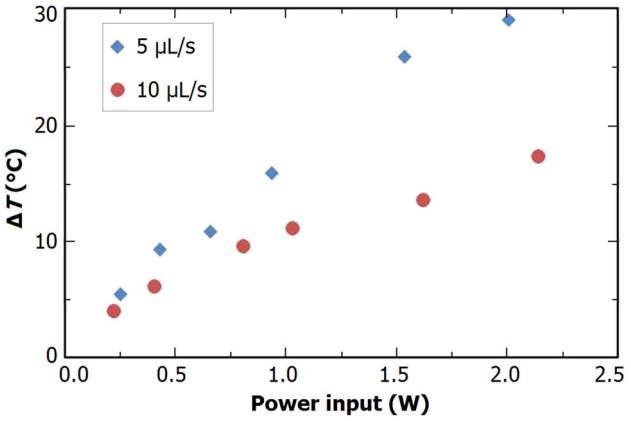

Fig. 7 Temperature changes (with respect to 25 °C) at the outlet of T-jump area as a function of power input

It should be noted that from the flow rates of 5 to 10 μL/s, the temperature increment is reduced almost by half at the same power input. Higher flow rate resulted in smaller T-jump owing to the reduction in time in which the fluid contacted with Pt heater. In addition, the heating rate could be up to 180 and 210 °C/s at the flow rates of 5 and 10 μL/s, respectively, for heater power ranging from 0.22 to 2.1 W.

4 Conclusion

We have demonstrated the development of a novel T-jump microfluidic chip which can be applied in synchrotron radiation measurements. Numerical simulation of T-jump microchannel and theoretical calculation of microheater were performed. Fluorescent dye showing a temperature-sensitive quantum yield was employed to determine the temperature characteristics of the microfluidic chip. The numerical and experimental results show that the proposed microfluidic chip has the characteristic of strong heat transfer ability to ensure the fast and effective heating-up of flowing solution with low thermal budget.

References

1. E.J. Crooks, The temperature-jump technique for the study of fast reactions in solution. J. Phys. E: Sci. Instrum. **16**, 1142–1147 (1983). doi:10.1088/0022-3735/16/12/003
2. Y. Hiragi, H. Nakatani, K. Kajiwara et al., Temperature-jump apparatus and measuring system for synchrotron solution X-ray-scattering experiments. Rev. Sci. Instrum. **59**, 64–66 (1988). doi:10.1063/1.1139967
3. Y. Hiragi, H. Inoue, Y. Sano et al., Dynamic mechanism of the self-assembly process of tobacco mosaic-virus protein studied by rapid temperature-jump small-angle X-ray-scattering using synchrotron radiation. J. Mol. Biol. **213**, 495–502 (1990). doi:10.1016/S0022-2836(05)80210-4
4. H. Neuweiler, M.C. Johnson, R.A. Fersht, Direct observation of ultrafast folding and denatured state dynamics in single protein molecules. Proc. Natl. Acad. Sci. U.S.A. **106**, 18569–18574 (2009). doi:10.1073/pnas.0910860106
5. T. Hart, P.L.L. Hosszu, R.C. Trevitt et al., Folding kinetics of the human prion protein probed by temperature jump. Proc. Natl. Acad. Sci. U.S.A. **106**, 5651–5656 (2009). doi:10.1073/pnas.0811457106
6. A.C. Dodson, N. Ferguson, J.T. Rutherford et al., Engineering a two-helix bundle protein for folding studies. Protein Eng. Des. Sel. **23**, 357–364 (2010). doi:10.1093/protein/gzp080
7. Y. Egozy, S. Weiss, T-jump apparatus with microwave heating. J. Phys. E: Sci. Instrum. **9**, 366–367 (1976). doi:10.1088/0022-3735/9/5/014
8. M. Kawakami, K. Akasaka, Microwave temperature-jump nuclear magnetic resonance system for aqueous solutions. Rev. Sci. Instrum. **69**, 3365–3369 (1998). doi:10.1063/1.1149102
9. J. Kubelka, Time-resolved methods in biophysics. 9. Laser temperature-jump methods for investigating biomolecular dynamics. Photochem. Photobiol. Sci. **8**, 499–512 (2009). doi:10.1039/b819929a
10. B.R. Dyer, J.S. Maness, S. Franzen et al., Hairpin folding dynamics: the cold-denatured state is predisposed for rapid refolding. Biochemistry **44**, 10406–10415 (2005). doi:10.1021/bi050698z
11. M.R. Ballew, J. Sabelko, M. Gruebele, Direct observation of fast protein folding: the initial collapse of apomyoglobin. Proc. Natl. Acad. Sci. U.S.A. **93**, 5759–5764 (1996). doi:10.1073/pnas.93.12.5759
12. B.D. Ferguson, R.T. Krawietz, F.J. Haw, Temperature-jump MAS NMR with a laser heater. J Magn Reason A **109**, 273–275 (1994). doi:10.1006/jmra.1994.1170
13. F. Tian, H.X. Li, Z.Y. Wang et al., Small angle X-ray scattering beamline at SSRF. Nucl. Sci. Tech. **26**, 030101 (2015). doi:10.13538/j.1001-8042/nst.26.030101
14. Y.T. Yang, W. Wen, Z.G. Yin et al., Introduction of the X-ray diffraction beamline of SSRF. Nucl. Sci. Tech. **26**, 020101 (2015). doi:10.13538/j.1001-8042/nst.26.020101
15. J. Sakakibara, J.R. Adrian, Whole field measurement of temperature in water using two-color laser induced fluorescence. Exp. Fluids **26**, 7–15 (1999). doi:10.1007/s003480050260
16. J.C.M. Coolen, N.R. Kieft, M.C.C. Rindt et al., Application of 2-D LIF temperature measurements in water using a Nd: YAG laser. Exp. Fluids **27**, 420–426 (1999). doi:10.1007/s003480050367
17. R. Fu, B. Xu, D. Li, Study of the temperature field in microchannels of a PDMS chip with embedded local heater using temperature-dependent fluorescent dye. Int. J. Therm. Sci. **45**, 841–847 (2006). doi:10.1016/j.ijthermalsci.2005.11.009
18. D. Ross, M. Gaitan, E.L. Locascio, Temperature measurement in microfluidic systems using a temperature-dependent fluorescent dye. Anal. Chem. **73**, 4117–4123 (2001). doi:10.1021/ac010370l
19. K.I.A. Lao, H.M.T. Lee, M.I. Hsing et al., Precise temperature control of microfluidic chamber for gas and liquid phase reactions. Sens Actuators **84**, 11–17 (2000). doi:10.1016/S0924-4247(99)00356-8
20. P. Zhang, H.X. Fu, Q.J. Wang et al., Research on micro-pt temperature sensor and its read-out circuit. Semicond. Technol. **37**, 464–469 (2012). doi:10.3969/j.issn.1003-353x.2012.06.012
21. T. Kozlova, M. Rudneva, W.H. Zandbergen, In situ TEM and STEM studies of reversible electromigration in thin palladium–platinum bridges. Nanotechnology **24**, 505708 (2013). doi:10.1088/0957-4484/24/50/505708